Applications and Applied Mathematics: An International Journal (AAM)

Volume 19 | Issue 1 Article 7

12-2023

# (R2058) MHD Stagnation Point Flow of Nanofluid with Buoyancy Effect Through a Porous Shrinking Sheet

Timothy L. Oyekunle
*University of Ilorin*

Mojeed T. Akolade
*University of Ilorin*

Samson A. Agunbiade
*Babcock University*

Paul O. Adeniran
*University of Ilorin*

Available at
http://pvamu.edu/aam
Appl. Appl. Math.
ISSN: 1932-9466
Vol. 19, Issue 1 (June 2024), 15 pages

Applications and Applied Mathematics:
An International Journal
(AAM)

# MHD Stagnation Point Flow of Nanofluid with Buoyancy Effect Through a Porous Shrinking Sheet

[1]**Timothy L. Oyekunle,** [2*]**Mojeed T. Akolade,** [3]**Samson A. Agunbiade and** [4]**Paul O. Adeniran**

[1,4] Department of Mathematics
University of Ilorin
Ilorin, Nigeria
[1]tloyekunle95@gmail.com
[4]femiadeniran92@gmail.com

[2] Department of Computer Science
Lead City University
Ibadan, Nigeria
[2*]akolade.mojeed@lcu.edu.ng
akolademojeed@yahoo.com

[3] Babcock University
Department of Basic Sciences
Ogun, Nigeria
[3]agunbiade1971@gmail.com

*Corresponding Author

## Abstract

The current investigation seeks to identify the response of buoyancy and heat source mechanisms on chemically reacting and magnetized nanofluid. The stagnation point flows through the shrinking porous surface assumed as an air-based fluid conveying nanoparticles under Buongiorno's model. This article contributes to the existing literature with the introduction of nonlinear convection of the nanofluid, triggered by the heat source, which accelerates the temperature of the fluid particles, thus resulting in airflow upstream. Subject to these conditions, the mathematical model is presented in PDE systems. An approach of similarity variable is employed to arrive at the ODE systems, which is then approximated via the collocation method with assumed Legendre functions of the first kind. The effect of various physical properties was obtained subsequently to the results when compared, validated, and illustrated through tables and graphs. The computed results show that a rise in the buoyancy parameter diminished the temperature and increased the velocity profiles. It is also displayed that the temperature is intensified with higher thermophoresis parameters and heat source values. The presence of thermophoresis shoots up the fluid concentration away from the wall surface but significantly affects the fluid concentration negatively near the surface.

**Keywords:** Nanofluid; Buoyancy; Thermophoresis; Chemical reaction; Legendre polynomial; shrinking surface

**MSC 2010 No.:** 65L60, 76A05, 76M55

# 1. Introduction

In a dynamical system, the stagnation point flow refers to the motion of a fluid in the closeness of a region at which the flow of the liquid is stationary, which is associated with an inviscid or potential flow. The study of stagnation point flow is essential because of its physical significance and a more comprehensive range of applications in sciences, engineering, etc. It is found relevant in the design of the bearing, wire drawings, plastic sheet drawings, electronic device cooling and polymer extrusion, etc. (Muhammad, 2019).

In view of its wide application range, researchers like Rakesh and Shilpa (2016) examined the effect of the magnetic field and quadratic on 2D stagnation point flow through a shrinking medium. It was noticed that the range of solution increases while examining quadratic convection parameters and magnetic field. Nirwana et al. (2020) studied the impact of heat transfer on stagnation point while flowing through a channel over a shrinking surface. From their study, it was observed that the range of solution increases with mass transfer. The response of MHD on the stagnation point flow of a nanofluid past a plate was carried out by Muhammad (2019). It was found that the presence of slip and magnetic parameters accelerated the velocity. A study on the electrically conducting flow of nanofluid subject to buoyancy effect was examined by Makinde et al. (2013). The influence of viscous dissipation and Joule heating on the MHD flow of micropolar fluid past an exponentially shrinking sheet was examined by Lund et al. (2020). It was revealed that triple solutions were obtained for non-Newtonian fluid and dual solutions for a Newtonian fluid. Based on MHD, Mohamad et al. (2019) presented stagnation point flow in a porous medium past a stretching/ shrinking sheet while investigating the effect of suction with stability analysis on heat transfer. The stagnation point flow of various classes of fluid on a shrinking surface for different geometries has attracted the attention of researchers like Yian et al. (2011), Bachok et al. (2013), Chrishnendu et al. (2014), Kamal et al. (2018), Lund et al. (2019), Rahman et al. (2019) to mention but a few.

The fluid containing nanoparticles, known as nanofluid, is an advanced heat transfer fluid that improves heat transfer by introducing nanoparticle materials with higher thermal conductivity characteristics. The novel properties of the fluid make it potentially useful in many industrial fields, such as refrigerators, engine cooling, electronic cancer therapeutics, domestic refrigerators, transportation, nuclear reactors, etc. (Nazar et al., 2004). In line with this importance, the MHD stagnation point flow of nanofluid with activation energy was dealt with by Muhammad et al. (2018). Their study shows that species concentration accelerates with the activation energy variable. Fahad and Muthtamilselvan (2020) analysed the response of thermophoresis with Brownian effect and micro-organisms on nanofluid's MHD. They concluded that the rise in temperature distribution increased the Brownian motion parameter. The effect of chemical reaction and dissipation on Casson nanofluid past a vertical porous plate was analysed by Oyekunle et al. (2021). Elelamy et al. (2020), Yusuf et al. (2020), and others also showed their interest in the importance of nanofluid flow through different geometries.

Patil and Kulkami (2019) stated some applications of nonlinear thermal and solutal convective flow that are useful when operating in industries, the field of engineering, and sciences. Researchers like Akolade et al. (2021a) and Idowu et al. (2021) examined the impact of quadratic convection on MHD Casson fluid flow through different geometries. It was recorded that a hike in nonlinear convection increases both velocity and temperature, while a decrease is realised in concentration fields. Ibrahim et al. (2017), Upadhya et al. (2018b), Nagaendramma et al. (2018), and Upadhya et al. (2018a), among others, revealed their interest in the impacts of the nonlinear convective flow of fluid through different geometries.

As a result of the relative scarcity of studies on the effects of buoyancy on chemically reacting MHD nanofluid stagnation point flow with a porous medium over a shrinking surface, the present work was motivated to perform thorough work in this particular area. Then, the dynamics flow problem was formulated by utilising the Collocation technique with the aid of assumed Legendre functions of the first kind. The present model is helpful in hydrology, heat exchangers, clothing science, the human body for the delivery of therapeutics, boosting exergy and minimising energy loss in the thermal system, and forestalling systems from overheating, among others.

## 2. Mathematical Analysis

The study considered a 2D laminar, incompressible, electrically conducting stagnation point flow of nanofluid flowing through a porous medium past a shrinking sheet, as shown in Figure 1. It is assumed that the fluid surface velocity and the free stream velocity are in the form $F_w\left(x^*\right) = bx^*$ and $F_e\left(x^*\right) \ = ax^*$, where $a$ and $b$ are constant, such that, $b>0$ and $b<0$ represents stretching and shrinking of the surface accordingly, and $a>0$ is the stagnation flow strength. The $x$-axis is taken along the direction of the shrinking surface, and the $y$-axis is perpendicular to it. This study neglected the role of generated magnetic field $B_0$ because it is assumed to be small. In contrast, the application of the uniform strength magnetic field $B_0$ is normal to the surface and parallel to the y-axis. $\theta^* = \theta^*_w$ and $\theta^* = \theta^*_\infty$ are taken to be the shrinking sheet and ambient temperatures, while $\phi^* = \phi^*_w$ and $\phi^* = \phi^*_\infty$ are the shrinking sheet and ambient concentrations respectively.

Based on the stated assumptions, and following the work of Rakesh and Shilpa (2016), Nirwana et al. (2020), and Fahad and Muthtamilselvan (2020), our model equations for the stagnation point flow of nanofluids consisting of continuity, momentum, and concentration equation becomes:

$$\frac{\partial f^*}{\partial x^*} + \frac{\partial g^*}{\partial y^*} = 0, \tag{1}$$

$$\begin{aligned} f^*\frac{\partial f^*}{\partial x^*} + g^*\frac{\partial f^*}{\partial y^*} = F_e\frac{\partial F_e}{\partial x^*} + \nu\frac{\partial^2 f^*}{\partial y^{*2}} + \left[\frac{\sigma B_0^2}{\rho} + \frac{\nu}{k}\right](F_e - f^*) \\ + g\left[\beta_0(\theta^* - \theta^*_\infty) + \beta_1(\theta^* - \theta^*_\infty)^2 + \beta_2(\phi^* - \phi^*_\infty) + \beta_3(\phi^* - \phi^*_\infty)^2\right], \end{aligned} \tag{2}$$

$$\begin{aligned} f^*\frac{\partial \theta^*}{\partial x^*} + g^*\frac{\partial \theta^*}{\partial y^*} = \alpha\frac{\partial^2 \theta^*}{\partial y^{*2}} + \tau\left[D_B\frac{\partial \phi^*}{\partial y^*}\frac{\partial \theta^*}{\partial y^*} + \frac{D_\theta}{\theta_\infty}\left(\frac{\partial \theta^*}{\partial y^*}\right)^2\right] \\ + \frac{\sigma B_0^2}{\rho c_p}(F_e - f^*)^2 + \frac{Q}{\rho c_p}(\theta^* - \theta^*_\infty), \end{aligned} \tag{3}$$

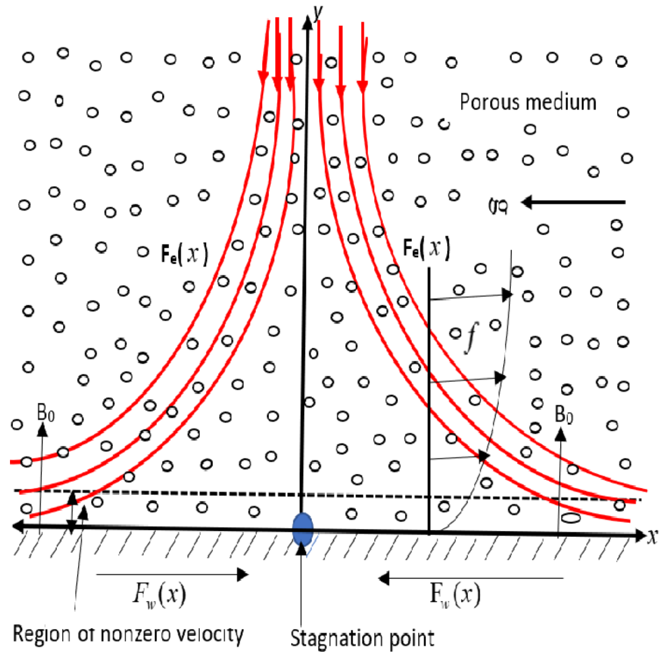


**Figure 1.** Model configuration of stagnation point flow.

$$f^*\frac{\partial \phi^*}{\partial x^*}+g^*\frac{\partial \phi^*}{\partial y^*}=D_B\frac{\partial^2 \phi^*}{\partial y^{*2}}+\frac{D_\theta}{\theta_\infty}\frac{\partial^2 \theta^*}{\partial y^{*2}}-k_1(\phi^*-\phi^*_\infty), \tag{4}$$

subjected to

$$\begin{aligned} &f^*=F_w(x^*),\ g^*=0\,,\ \theta^*=\theta^*_w(x^*),\ \phi^*=\phi^*_w(x^*)=\phi^*_\infty+dx^* \ \text{ at }\ y^*=0,\\ &f^*\to F_e(x^*)\ ,\ \ \theta^*\to\theta^*_\infty\ ,\ \ \phi^*\to\phi^*_\infty \quad \text{as}\ \ y^*\to\infty, \end{aligned} \tag{5}$$

where $\alpha$ and $g$ are the thermal diffusivity and acceleration due to gravity, respectively; $\beta_0$ and $\beta_1$ are the coefficient of thermal expansion, respectively; $D_B$ and $B_0$ are the Brownian diffusion coefficient and applied magnetic field, respectively; $\tau$ is the ratio of the heat capacity of the nanoparticle to the base fluid, $f^*$ and $g^*$ are the velocity component in the directions of $x$ and $y$, respectively; $k_1$ and $Q$ are the chemical reaction constant and heat source/sink, respectively; $\mu$ is the coefficient of viscosity, $\beta_3$ and $\beta_4$ are the coefficient of solutal expansion, respectively; $\rho$ and $D_\theta$ are the density and thermophoresis diffusion coefficient, respectively; $\nu=\frac{\mu}{\rho}$ is the kinematic viscosity, $\theta^*$and $\phi^*$ are the fluid temperature and fluid concentration, respectively; $k$ is the permeability of the porous medium.

Introduction of the stream function $f^*=\frac{\partial\psi}{\partial y^*},\ g^*=-\frac{\partial\psi}{\partial x^*}$ and employing the following similarity transformation,

$$\eta=\left(\frac{F_e}{\nu x^*}\right)^{\frac{1}{2}}y^*,\quad \psi=(a\nu)^{\frac{1}{2}}x^*f(\eta),\quad \theta(\eta)=\frac{\theta^*-\theta^*_w}{\theta^*_w-\theta^*_\infty},\quad \phi(\eta)=\frac{\phi^*-\phi^*_w}{\phi^*_w-\phi^*_\infty}, \tag{6}$$

then, Equations (1) through (5) are reduced to a simpler form. By simplification, the following nonlinear differential equations were obtained:

$$f'''(\eta) + f(\eta)f''(\eta) - [f'(\eta)]^2 + (H+B)[1-f'(\eta)] \\ + \alpha\theta(\eta)[1-\gamma\theta(\eta)] + \beta\phi(\eta)[1-\delta\phi(\eta)] + 1 = 0, \tag{7}$$

$$\theta''(\eta) + P_r\,[f(\eta)\,\theta'(\eta) - \theta(\eta)\,f'(\eta)] + N_b\,\phi'(\eta)\,\theta'(\eta) + N_t\,(\theta'(\eta))^2 \\ + HP_rE_c\,[1 - 2\,f'(\eta) + (f'(\eta))^2] + P_r\,\varepsilon\,\theta(\eta) = 0, \tag{8}$$

$$\phi''(\eta) + S_c\,[f(\eta)\,\phi'(\eta) - \phi(\eta)\,f'(\eta) - G\,\phi(\eta)] + \frac{N_t}{N_b}\,\theta''(\eta) = 0, \tag{9}$$

with boundary conditions

$$\begin{cases} f(\eta)=0, \;\; f'(\eta) = \frac{b}{a} = Z, \;\; \theta(\eta)=1, \;\; \phi(\eta)=1 \quad \text{at} \;\; \eta = 0, \\ f'(\eta) \to 1, \;\; \theta(\eta) \to 0, \;\; \phi(\eta) \to 0 \quad \text{as} \;\; \eta \to \infty, \end{cases} \tag{10}$$

where

$$\left.\begin{array}{l} H = \frac{\sigma B_0^2}{\rho a}, \; B = \frac{\nu}{ak}, \; Gt_{x^*} = \frac{g\beta_0(\theta_w^* - \theta_\infty^*)x^{*3}}{\nu^2}, \; Re_{x^*} = \frac{x^* F_e}{\nu}, \; \lambda = \frac{Gr_{x^*}}{Re_{x^*}^2}, \; \gamma = \frac{\beta_1}{\beta_0}(\theta_w^* - \theta_\infty^*), \\ Gc_{x^*} = \frac{g\beta_2(\phi_w^* - \phi_\infty^*)x^{*3}}{\nu^2}, \; \delta = \frac{\beta_3}{\beta_2}(\phi_w^* - \phi_\infty^*), \; N_b = \frac{\tau D_B(\phi_w^* - \phi_\infty^*)}{\alpha}, \; N_t = \frac{\tau D_{\theta^*}(\theta_w^* - \theta_\infty^*)}{\theta_\infty^* \alpha} \\ \tau = \frac{\rho c_p}{\rho c_f}, \; E_c = \frac{(ax^*)^2}{c_p(\theta_w^* - \theta_\infty^*)}, \;\; \varepsilon = \frac{Q}{\rho c_p}, \;\; S_c = \frac{\nu}{D_B}, \;\; G = \frac{k_1}{a}, \;\; Z = \frac{b}{a}, \; P_r = \frac{\nu}{\alpha}, \; \beta = \frac{Gc_{x^*}}{Re_{x^*}^2}, \end{array}\right\} \tag{11}$$

such that: $G$, $P_r$ represent the chemical reaction parameter and Prandtl number, $H$ represents the magnetic field, $\mathrm{Re}_x{}^*$ represents the Reynolds number, B represents the permeability parameter, $\delta$ and $\mathrm{N}_b$ are the solutal nonlinear parameter and Brownian motion parameter, respectively; Schmidt number ($\mathrm{S}_c$), magnetic field (H), $\mathrm{Gt}_x{}^*$ and $\mathrm{Gc}_x{}^*$ are Grashof numbers, respectively; $\alpha$ and $\beta$ are the buoyancy parameters, respectively; Reynolds number ($\mathrm{Re}_x{}^*$), $\tau$ represents ratio of the heat capacity of nanoparticle to the base fluid, $\mathrm{E}_c$ represents the Eckert number, $\varepsilon$ and Z are the heat source/sink parameter and velocity ratio parameter, respectively; $\mathrm{N}_t$ and $\gamma$ are the thermophoresis parameter and thermal nonlinear parameter, respectively.

## 2.1. Flow characteristics

As a result of practical applications of flow characteristics, the following physical parameters $C_f$, $Nu_{x^*}$, and $Sh_{x^*}$ are defined:

$$C_f = \frac{\mu\left(\frac{\partial f^*}{\partial y^*}\right)_{y^*=0}}{\rho F_e^2}, \quad Nu_{x^*} = \frac{-x^*\left(\frac{\partial \theta^*}{\partial y^*}\right)_{y^*=0}}{(\theta_w^* - \theta_\infty^*)} \quad \text{and} \quad Sh_{x^*} = \frac{-x^*\left(\frac{\partial \phi^*}{\partial y^*}\right)_{y^*=0}}{(\phi_w^* - \phi_\infty^*)}. \tag{12}$$

The following flow characteristics were obtained while applying Equation (6) to Equation (12):

$$C_f Re_{x^*}^{1/2} = f''(0), \quad Nu_{x^*} Re_{x^*}^{-1/2} = -\theta'(0), \quad Sh_{x^*} Re_{x^*}^{-1/2} = -\phi'(0), \tag{13}$$

where $Re_x = \frac{F_e x}{\nu}$ denotes Reynolds number.

## 3. Method of Solution

Numerous researchers have proven the accuracy of the Collocation Method. The approach is easy to use, efficient, and rapid convergence in estimating systems of PDEs and ODEs. The CCM is fully documented in the works of Idowu et al. (2021), Babatin (2018), Parand et al. (2017), Akolade et al. (2021b), Uddin et al. (2018), Mallawi et al. (2019), and Javed and Mustafa (2016). Further studies on this collocation include the work of Kürkçü (2021) and Adel et al. (2021), where a matrix Bernoulli polynomial is constructed with the implementation of the collocation method.

In this section, the solution to Equations (7) through (9) subjected to the boundary condition (10) was obtained via the Legendre collocation method with polynomial as the basis function. Also, the interval $[0, \infty)$ is truncated while employing the domain truncation approach $[0, L]$. Through the following algebraic mapping:

$$\xi = \frac{2\eta}{\mathrm{L}} - 1, \qquad \xi \in [-1, 1], \tag{14}$$

the interval [0, L] is transformed to [-1,1] as defined on the Legendre polynomial. The scaling parameter L is assumed sufficiently large relative to the boundary layer thickness (Olagunju et al (2013), Aysun and Sali (2013)).

Employing the Legendre polynomial $p_j(\eta)$, the unknown functions $f(\eta)$, $\theta(\eta)$and $\phi(\eta)$ are approximated to give a sum of a finite series:

$$f(\eta)\approx f_N(\xi) = \sum_{j=0}^{N} a_j p_j(\eta), \quad \theta(\eta)\approx\theta_N(\xi) = \sum_{j=0}^{N} b_j p_j(\eta), \quad \phi(\eta)\approx\phi_N(\xi) = \sum_{j=0}^{N} c_j p_j(\eta), \tag{15}$$

where $j= 0, 1, ..., N$ Newton iteration technique is used with MATHEMATICA 11.0 symbolic package to generate the 3N+3 algebraic system and determine the 3N+3 unknown coefficients ($a_j$, $b_j$ and $c_j$), which are then substituted back into equation (15) as an approximate solution.

## 4. Results and Discussion

Here, numerical results for the flow field and characteristics solutions were obtained while solving the differential equations (7) through (9) subject to the boundary condition (10) through the use of the Legendre collocation method with a polynomial as the basis function. For clarity, the effects of important parameters involved in the flow distributions are shown in Figures 2 through 13. The numerical results of this work are obtained based on the following fixed data $\alpha$=0.5, Nt=0.1, $\delta$=0.5, $\beta$=0.5, H=0.5, B=0.5, $\varepsilon$=0.5, Sc=1.0, G=0.5, Ec=0.1, Nb=0.1, Z= -1.0, Pr =1.0 and $\gamma$=0.5 as used by Rakesh and Shilpa (2016) and Nirwana et al. (2020), except otherwise stated. The Skin friction coefficient is tabulated in Table 1, and the result was found to be in excellent agreement when compared with those of Wang (2008), Rakesh and Shilpa (2016), and Nirwana et al. (2020) while setting the embedded parameters to zero with different values of Z for Pr=1.

Apparently, the effect of the Buoyancy parameter $\alpha$ and $\beta$ on (a) velocity and (b) temperature distributions is shown in Figures 2 and 3. We noticed that a hike in Buoyancy parameters $\alpha$ and $\beta$

**Table 1.** Comparison of the Skin friction $f''(0)$ values with respect to Z when $\alpha$, $\gamma$, $\delta$, $\beta$, H, B, G, $\varepsilon$, Sc, Nt, Ec, Nb are set to zero and Pr=1.

| $Z$ | Rakesh and Shilpa (2016) | Nirwana et al. (2020) | Wang (2008) | Present results |
|---|---|---|---|---|
| -0.25 | 1.402253 | 1.402241 | 1.40224 | 1.40224 |
| -0.50 | 1.495685 | 1.49567 | 1.49567 | 1.49567 |
| -0.75 | 1.489316 | 1.489299 | 1.4893 | 1,4893 |
| -1.0 | 1.328840 | 1.328819 | 1.32882 | 1.32882 |
| -1.15 | 1.082262 | 1.082244 | 1.08223 | 1.08223 |
| -1.20 | 0.932512 | - | - | 0.932474 |
| -1.2465 | - | 0.584295 | 0.5843 | 0.584356 |
| 0 | 1.2325975 | 1.232588 | 1.232588 | 1.23259 |
| 0.1 | 1.1465699 | 1.146561 | 1.146560 | 1.146560 |
| 0.2 | 1.0511379 | 1.051130 | 1.051130 | 1.051130 |
| 0.5 | - | 0.713294 | 0.71330 | 0.713295 |
| 2.0 | -1.887316 | -1.887307 | -1.88730 | -1.88731 |
| 5.0 | -10.26479 | -10.264749 | -10.26475 | -10.26470 |

accelerated velocity and diminished temperature profiles. Physically, a decrease in the fluid temperature $\theta(\eta)$ causes an increase in fluid density $\rho$. Therefore, the buoyancy in the fluid, which is directly proportional to the density, increased at the cooling buoyancy rate. Figure 4 displays the dependence of the magnetic field (H) on temperature and velocity distribution profile. The presence of $H$ reduces the $\theta(\eta)$ and accelerates the momentum field accordingly. Physically, Lorentz's force tends to improve the fluid velocity due to the nature of the velocity ratio of the fluid. Without repetition, the same behavior observed in Figure 4 is also experienced in Figure 5 (a and b) while taking into consideration the variation of porosity parameter (B) with the velocity and temperature distributions.

The influence of quadratic thermal convection ($\gamma$) on energy and velocity distribution is profiled in Figure 6. We identified that increasing the thermal convection ($\gamma$) accelerates the temperature and diminishes the velocity profiles. Physically, to predict an accurate transfer of heat and mass across the flow field, thermal conductivity material needs to be improved for the convection process. Figure 7 (a and b) presents the influence of heat source parameters on $\theta(\eta)$and $\varphi(\eta)$ profiles. It is realized that higher values of the heating parameter $\varepsilon$ diminished the $\varphi(\eta)$ and accelerated the temperature $\theta(\eta)$ distributions. Naturally, the temperature tends to rise due to the absorption of heat. The response Ec on the $\varphi(\eta)$ and $\theta(\eta)$ distribution is shown in Figure 8. An increase in the temperature and a decrease in the concentration distributions is noticed with a hike in the Eckert number. Figure 9 shows variation in $Pr$ with temperature $\theta(\eta)$ and $\varphi(\eta)$ profiles. The results show that with a rise in the Prandtl number Pr, the $\theta(\eta)$ distribution rises to a particular point on the flow field and then decreases. At the same time, the reverse is the case in the behavior of the $\varphi(\eta)$ profile.

Figure 10 portrays the response of Nb on $\theta(\eta)$ and $\varphi(\eta)$ profiles. It is seen that with a rise in Brownian motion, the temperature profile accelerated while concentration rose to a particular point on the flow field and then declined. Naturally, the collision caused by nanofluid particles due to a hike in the Brownian motion generates thermal energy, which speeds up the temperature profiles. The impact of $Nt$ on $\theta(\eta)$ and $\varphi(\eta)$ distributions is depicted in Figure 11. It is discovered that the temperature is enhanced with an increase in Nt. In the case of concentration profiles, a decrease is first noticed before an increase with a rise in $Nt$. The influence of velocity ratio $(Z)$ on temperature and nanoparticle fraction $\varphi(\eta)$ is displayed in Figure 12. The decrease in the velocity ratio gives rise to temperature distributions, while the nanoparticle volume fraction decreases with Z to a particular point on the flow field and then increases. The effect of $G$ and $Sc$ on the nanoparticle volume fraction $\varphi(\eta)$ is presented in Figure 13a. The observations in Figure 13a show that a hike in $Sc$ slows down the concentration profiles. Physically, a rise in Schmidt's number entails a reverse trend in molecular diffusion. Likewise, in Figure 13b, a higher value of chemical reaction accelerated the mass transfer as a result of destructive chemicals. It diminished the concentration profiles due to an increase in mass transfer and the Solutal boundary layer thickness reduction as a result of destructive chemicals.

## 5. Conclusion

In this paper, numerical solutions have been obtained to investigate MHD nanofluid stagnation flow over a shrinking plate in a porous medium with the presence of buoyancy and heat sources. Governing partial differential equations were transformed into sets of nonlinear differential equations using a similarity variable. The transformed equations governing the fluid flow were solved while employing the collocation method with the aid of assumed Legendre functions of the first kind. The solution to the equations was obtained using MATHEMATICA 11.0 software. Numerical results were obtained for the effect of various parameters of interest on the fluid flow characteristics. Thereby, tables and graphs are presented and discussed. With respect to the present investigations, the following observations are made:

(1) Flow momentum is accelerated, and the energy field diminished with injection in buoyancy, magnetic field, and Darcy parameters, while a hike in nonlinear thermal convection ($\gamma$) slowdown the velocity $f^{'}(\eta)$ and speedup the temperature profiles;
(2) An increase in heat source parameter ($\epsilon$) and Eckert number ($Ec$) retard the nanoparticle volume fraction but gave rise to the temperature field;
(3) The temperature profile rises with Brownian motion ($Nb$), while concentration is elevated to a particular point on the flow field and then declined;
(4) The temperature distributions rise with the thermophoresis parameter ($Nt$) and decrease to a particular point before an increase is observed for concentration profiles;
(5) The higher values of the velocity ratio reduce the temperature distributions, while the nanoparticle volume fraction $\tau$ increases with Z to a particular point on the flow field and then decreases;
(6) A hike in Schmidt number ($Sc$) slowed down the concentration profiles, and a higher value of chemical reaction ($G$) diminished the concentration profiles.

# REFERENCES


Adel, W., Biçer, K. E. and Sezer, M. (2021). A novel Numerical approach for simulating the nonlinear MHD Jeffery–Hamel flow problem, International Journal of Applied and Computational Mathematics, Vol. 7, Article No. 74. https://doi.org/10.1007/s40819-021-01016-3

Akolade, M.T., Adeosun, T.A. and Olabode, J.O. (2021b). Influence of thermophysical features on MHD squeezed flow of dissipative Casson fluid with chemical and radiative effects, Journal of Applied and Computational Mechanics, Vol. 7, Issue 4, pp. 1999-2009.

Akolade, M.T., Idowu, A.S. and Adeosun, A.T. (2021). Multislip and Soret-Dufour influence on nonlinear convection flow of MHD dissipative Casson fluid over a slendering stretching sheet with generalized heat flux phenomenon, Heat. Trans. Res., Vol. 50, Issue 4, pp. 3913-3933.

Aysun, G. and Salih, Y. (2013). Legendre collocation method for solving nonlinear differential equations, Math. Comput. Appl., Vol. 18, No. 3, pp. 521-530.

Babatin, M.M. (2018) Numerical treatment for the flow of Casson fluid and heat transfer model over an unsteady stretching surface in the presence of internal heat generation/absorption and thermal radiation, Applications and Applied Mathematics: An International Journal (AAM), Vol. 13, Issue 2, Article 16, pp. 854-862.

Bachok, N., Ishak, A., Nazar, R. and Senu, N. (2013). Stagnation point flow over a permeable stretching/shrinking sheet in a copper water nanofluid, Boundary Value Problems, Article 39.

Chrishnendu, B., Layek, G.C. and Seth, G.S. (2014). Soret and Dufour effect on convective heat and mass transfer in stagnation point flow toward a shrinking surface, R. Swedish Acad. Sci., Vol. 89, pp. 1-10.

Elelamy, A.F., Elgazery, N.S. and Ellahi, R. (2020). Blood flow of MHD non-Newtonian nanofluid with heat transfer and slip effects: Application of bacterial growth in heart valve, Int. J. Numer. Methods Heat Fluid Flow, Vol. 30, No. 11, pp. 4883-4908.

Fahad, A. and Muthtamilselvan, M. (2020). Stagnation point flow of nanofluid containing Microorganisms, Case Studies in Thermal Engineering, Vol. 21.

Idowu, A.S., Akolade, M.T., Oyekunle, T.L. and Abubakar, J.U. (2021). Nonlinear convection flow of dissipative Casson nanofluid through an inclined annular microchannel with a porous medium, Heat Trans. Res., Vol. 50, Issue 4, pp. 3388-3406.

Javed, T. and Mustafa, I. (2016). Slip effects on a mixed convection flow of a third-grade fluid near the orthogonal stagnation point on a vertical surface, Journal of Applied Mechanics and Technical Physics, Vol. 57, pp. 527-536.

Kamal, F., Khalry, Z., Anuar, I. and Loan, P. (2018). Stability analysis on the stagnation point flow and heat transfer over a permeable stretching/shrinking sheet with heat source effect, International Journal of Numerical Methods for Heat and Fluid Flow, Vol. 28, pp. 2650-2663.

Kürkçü, Ö.K. (2021). A numerical solution of MHD Jeffery-Hamel model arising in fluid mechanics, 7th International IFS and Contemporary Mathematics Conference, Mersin, Turkey, pp. 177-183.

Lund, L.A., Zurni, O. and Ilyas, K. (2019). Quadruple solutions of mixed convection flow of magnetohydrodynamic nanofluid over exponentially vertical shrinking and stretching surfaces:

Stability analysis, Computer Methods and Programs in Biomedicine, Vol. 182.

Lund, L.A., Zorni, O., Ilyas, K., Jaward, R., El-Sayed, M.S. and Asiful, H.S. (2020). Magnetohydrodynamic (MHD) flow of micropolar fluid with effect of viscous dissipation and joule heating over an exponential shrinking sheet: Triple solutions and stability analysis, Symmetry, Vol. 12, No. 1, 142. https://doi.org/10.3390/sym12010142

Makinde, O.D., Khan, W.A. and Khan, Z.H. (2013). Buoyancy effects on MHD stagnation point flow and heat transfer on a nanofluid past a convectively heated stretching/shrinking sheet, International Journal of Heat and Mass Transfer, Vol. 62, No. 1, pp. 526-533.

Mallawi, F., Alzaidy, J. and Hafez, R. (2019). Application of a Legendre collocation method to the space–time variable fractional-order advection–dispersion equation, Journal of Taibah University for Science, Vol. 13, No. 1, pp. 324-330.

Muhammad, A.S. (2019). MHD stagnation point flow of Nanofluid on a plate with Anisotropic slip, Symmetry, Vol. 11, No. 2, 132. doi:10.3390/sym11020132

Muhammad, I.K., Tasawar, H., Muhammad, I.K. and Alsaedi, A. (2018). Activation energy impact in nonlinear radiative stagnation point flow of cross nanofluid, Int. Commun. Heat Mass Tran., Vol. 91, pp. 216-224.

Nasar, R., Amin, N., Filip, D. and Pop, I. (2004). Unsteady boundary layer flow in the region of the stagnation point on a stretching sheet, Int. J. Eng. Sci., Vol. 42, pp. 1241-1253.

Nirwana, J., Haliza, R. and Norfifah, B. (2020). Suction effect on stagnation point flow and heat transfer over an exponentially shrinking sheet in a porous medium, Journal of Advanced Research in Fluid Mechanics and Thermal Sciences. https://doi.org/10.37934/arfmts.73.2.163174

Noormaizatulnazuha, M., Kamal, F. and Zalmi, K. (2019). Effect of suction on the stagnation point flow and heat transfer over a stretching/shrinking sheet in a porous medium with stability analysis, Applied Mathematics and Computational Intelligence, Vol. 8, No. 1, pp. 17-30.

Olagunju, A.S., Joseph, F.L. and Raji, M.T. (2013). Comparative study of the effect of different collocation Points on Legendre-collocation method of solving second-order boundary value problems, IQSR J. Math, Vol. 7, Issue 2, pp. 35-41.

Oyekunle, T.L., Akolade, M.T. and Agunbiade, S.A. (2021). Thermal-diffusion and diffusion-thermo effects on heat and mass transfer in chemically reacting MHD Casson nanofluid with viscous dissipation, Int. J. Application and Applied Mathematics, Vol. 16, Issue 1, pp. 705-723.

Parand, K., Ghaderi, A., Yousefi, H. and Delkhosh, M. (2017). Solving magneto-hydrodynamic squeezing flow between two parallel disks with suction or injection using three classes of polynomials, Palestine Journal of Mathematics, Vol. 6, pp. 333-347.

Patil, P.M. and Kulkami, M. (2021). Nonlinear mixed convective nanofluid flow along moving vertical rough plate, Revista Mexican Fisica, Vol. 66, No. 2, pp. 135-161.

Rahmam, A.N.H., Bachok, N. and Rosali, H. (2019). Numerical solutions of MHD stagnation point flow over an exponentially stretching/shrinking sheet in a nanofluid, Int. Journal of Physics: Conference Series, Vol. 1366, No. 1, p.012012.10p.

Rakesh, K. and Sood, S. (2016). Interaction of magnetic field and non linear convection in the stagnation point flow over a shrinking sheet, Journal of Engineering. htttp://dx.doi.org/10.1155/2016/6752520

Uddin, M., Kabir, M., Bég, O.A. and Alginahi, Y. (2018) Chebyshev collocation computation of magneto-bioconvection nanofluid flow over a wedge with multiple slips and magnetic induction, Proceedings of the Institution of Mechanical Engineers, Part N: Journal of Nanomaterials, Nanoengineering and Nanosystems, Vol. 232, Issue 4, pp. 109-22.

Yian, L.Y., Ishak, A. and Pop, I. (2011). Stagnation point flow with suction towards a shrinking sheet, Sains Malaysiana, Vol. 40, No. 10, pp. 1179-1186.

Yusuf, T.A., Adesanya, S.O. and Gbadeyan, J.A. (2020). Entropy generation in MHD Williamson nanofluid over a convectively heated stretching plate with chemical reaction, Heat Transfer, Vol. 49, Issue 4, pp. 1982-1999.

## Appendix

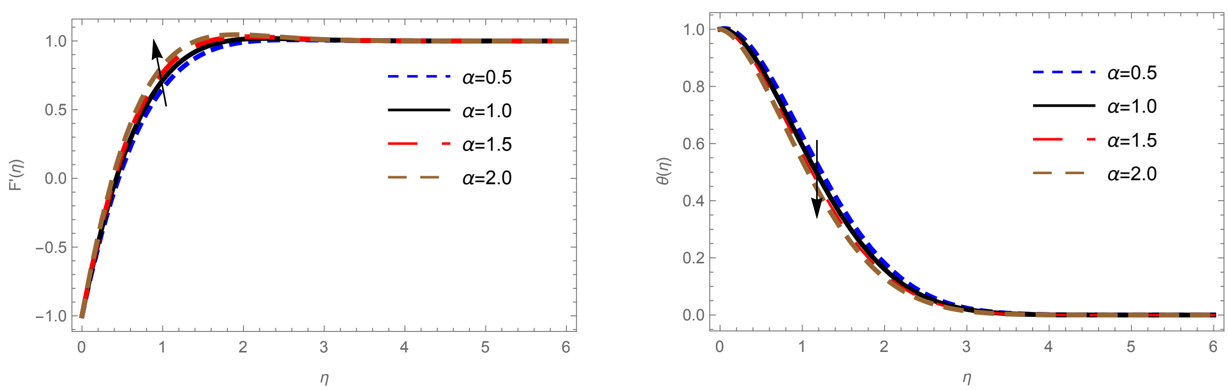


**a** **b**

**Figure 2.** Buoyancy parameter ($\alpha$) influence on $f'(\eta)$ and $\theta(\eta)$ profiles

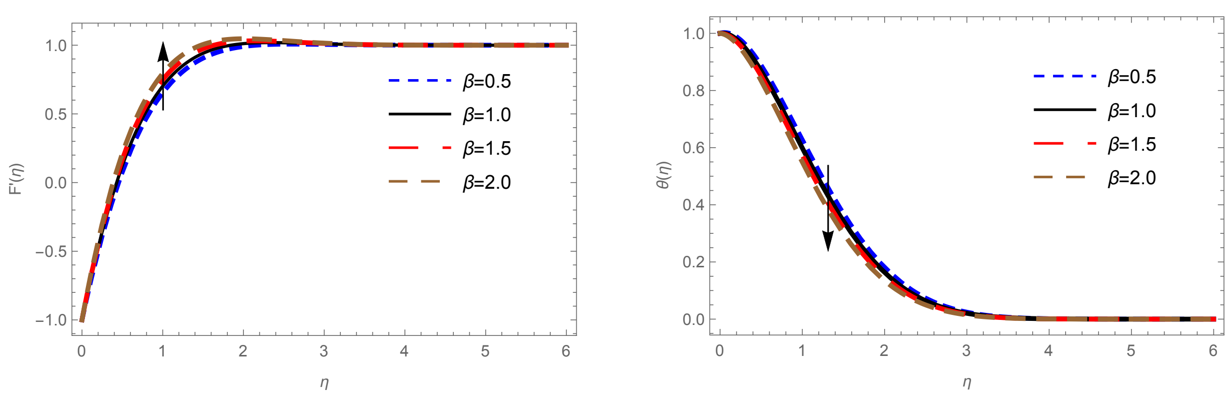


**a** **b**

**Figure 3.** Buoyancy parameter ($\beta$) influence on $f'(\eta)$ and $\theta(\eta)$ profiles

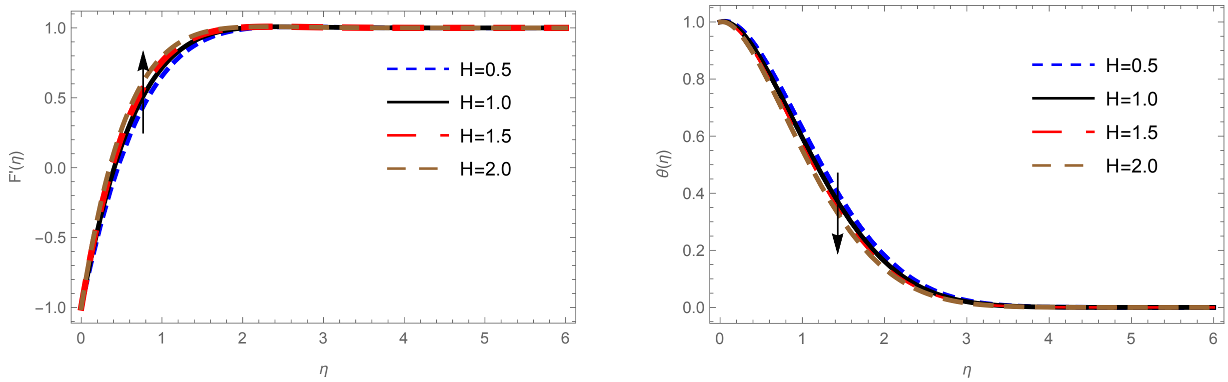


**a** **b**

**Figure 4.** Magnetic field $(H)$ influence on $f'(\eta)$ and $\theta(\eta)$ profiles

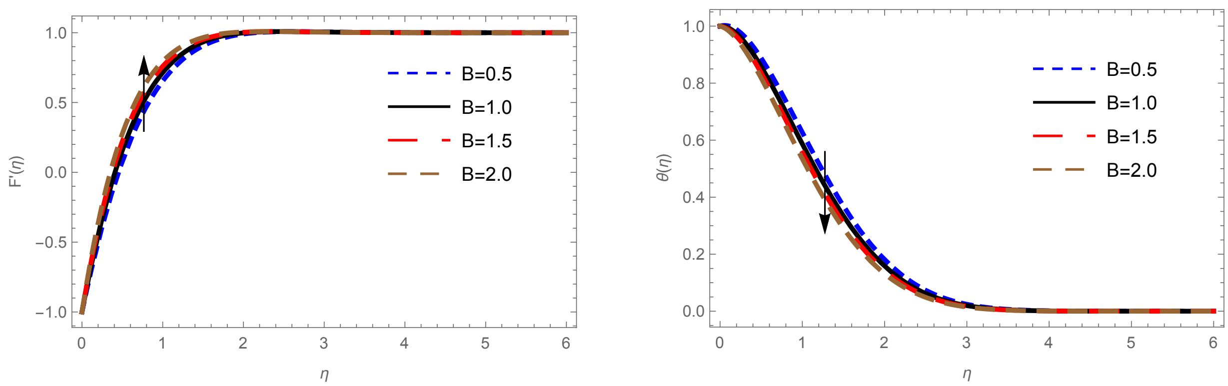


**a** **b**

**Figure 5.** Porosity parameter $(B)$ effect on $f'(\eta)$ and $\theta(\eta)$ profiles

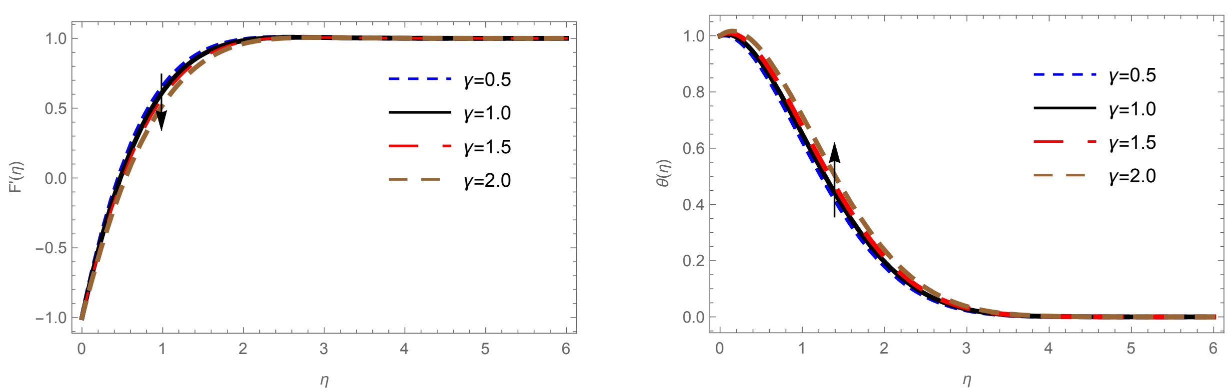


**a** **b**

**Figure 6.** Nonlinear thermal convection $(\gamma)$ influence on $f'(\eta)$ and $\theta(\eta)$ profiles

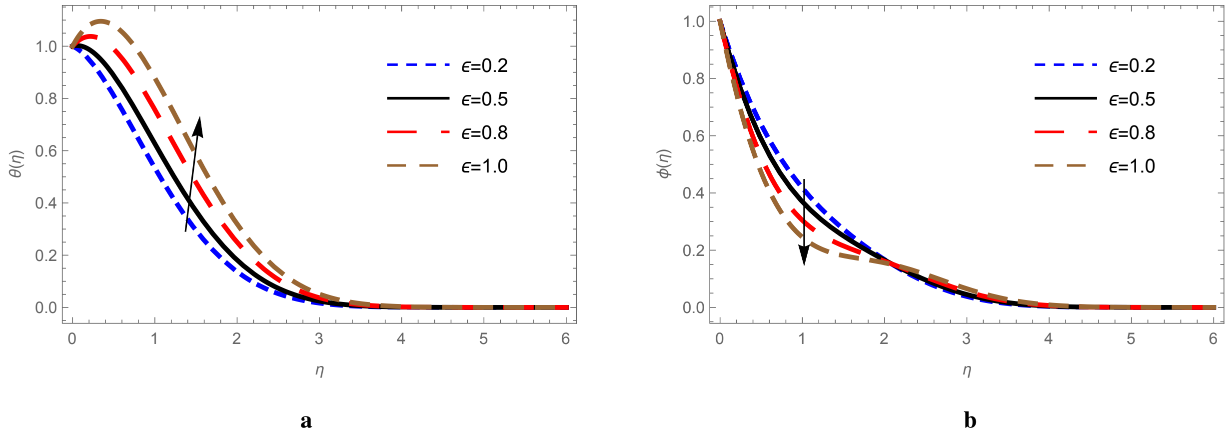


**Figure 7.** Impact of Heat source parameter ($\varepsilon$) on $\theta(\eta)$ and $\varphi(\eta)$ distributions

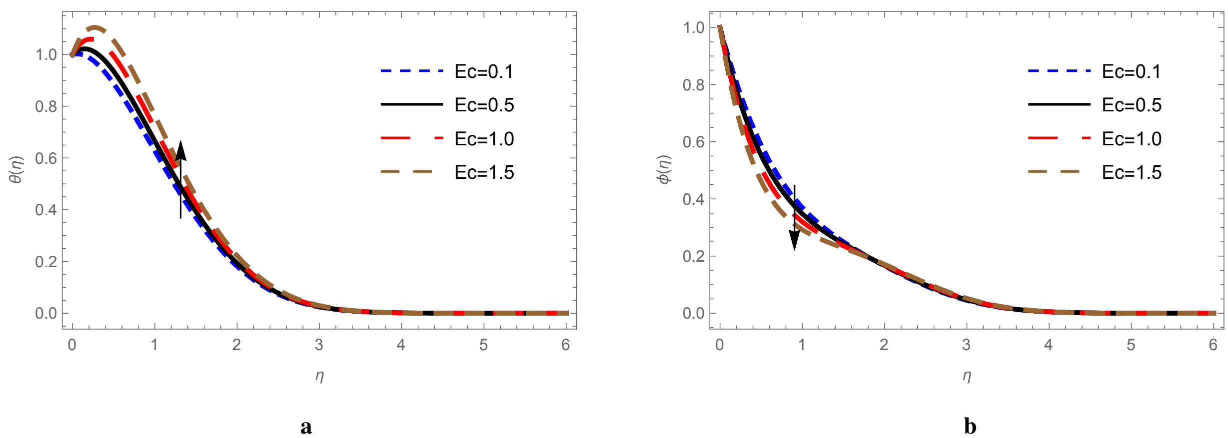


**Figure 8.** Eckert number $Ec$ response on $\theta(\eta)$ and $\varphi(\eta)$ distributions

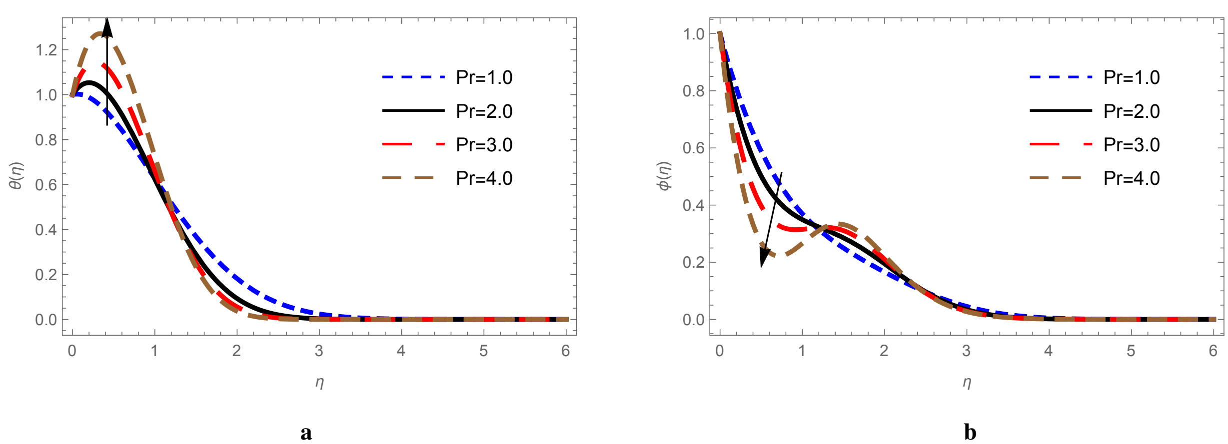


**Figure 9.** Influence of Pr on $\theta(\eta)$ and $\varphi(\eta)$ distributions

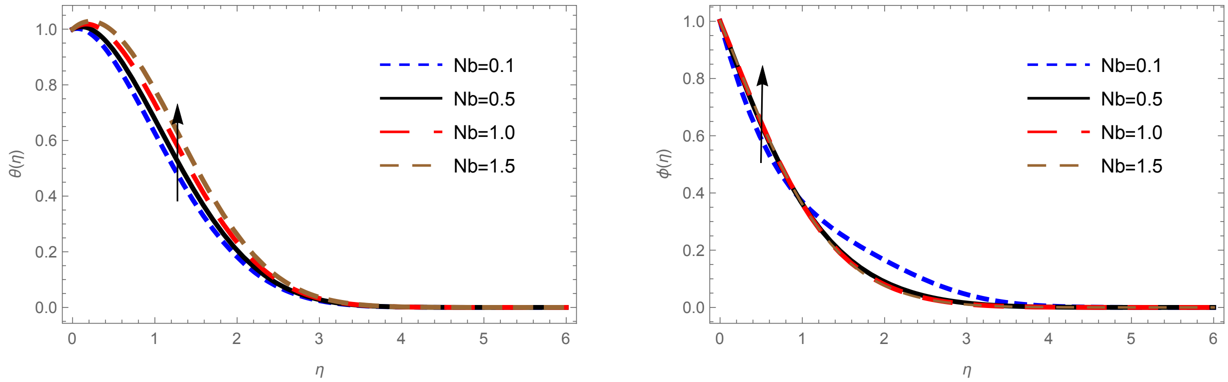


a b

**Figure 10.** Influence of $Nb$ on $\theta(\eta)$ and $\varphi(\eta)$ distributions

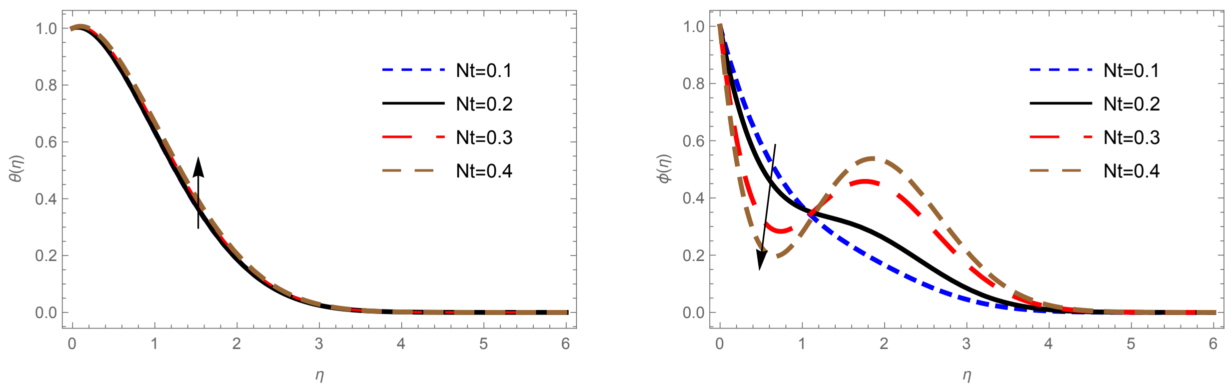


a b

**Figure 11.** Thermophoresis parameter (Nt) parameter on $\theta(\eta)$ and $\varphi(\eta)$ distributions

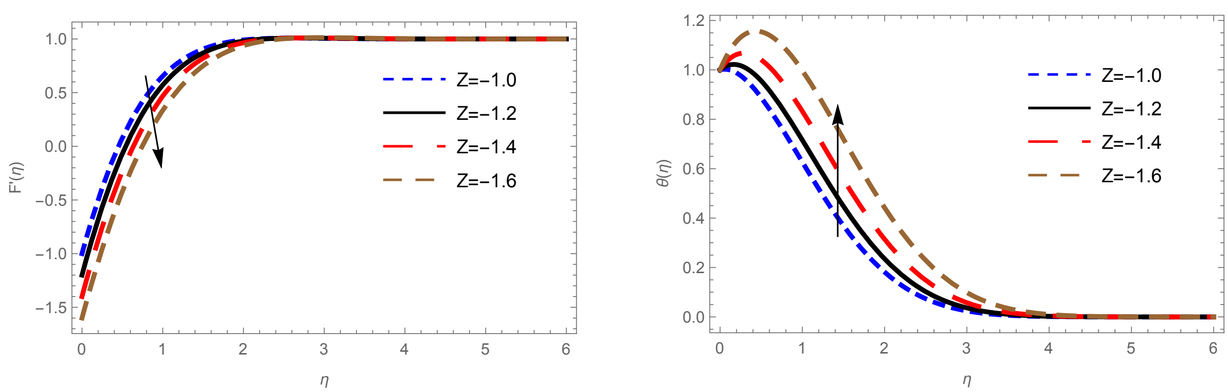


a b

**Figure 12.** Velocity ratio parameter $(Z)$ influence on $\theta(\eta)$ and $\varphi(\eta)$ distributions

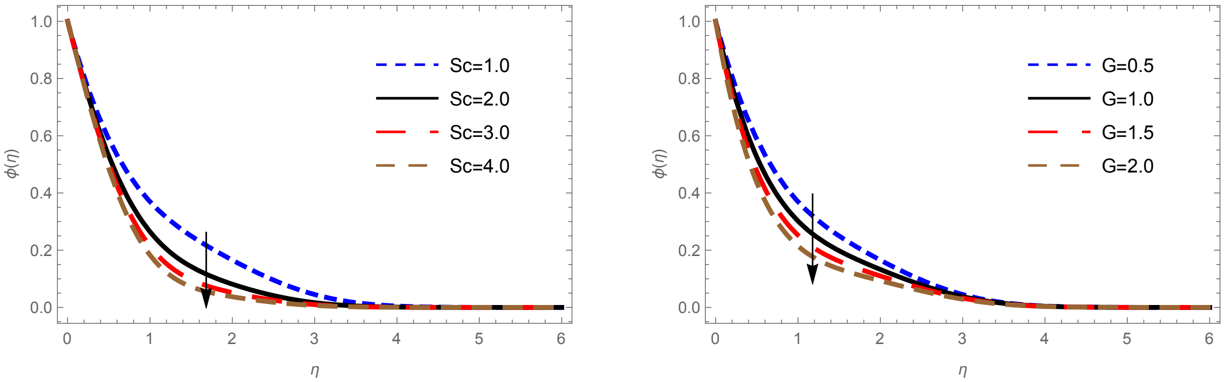


**a** **b**

**Figure 13.** Influence of $G$ and $Sc$ and on $\varphi(\eta)$ profiles

**Table 2.** Computational values of Skin friction $f''(0)$, Nusselt number $\theta'(0)$, and Sherwood number $-\varphi(0)$ with involved parameters of the problem

| H | Pr | Ec | G | Nb | Nt | $\alpha$ | B | -Z | Sc | $\gamma$ | $\delta$ | $\epsilon$ | B | $f''(0)$ | $\theta'(0)$ | $-\varphi(0)$ |
|---|---|---|---|---|---|---|---|---|---|---|---|---|---|---|---|---|
| 0.5 | 1.0 | 0.1 | 0.5 | 0.1 | 0.1 | 0.5 | 0.5 | 1.0 | 1.0 | 0.5 | 0.5 | 0.5 | 0.5 | 2.76094 | 0.08843 | 1.08604 |
| 1.0 | | | | | | | | | | | | | | 3.10851 | 0.06938 | 1.12281 |
| | 1.2 | | | | | | | | | | | | | 2.75921 | 0.17595 | 1.17899 |
| | | 0.5 | | | | | | | | | | | | 2.75946 | 0.31204 | 1.28542 |
| | | | 0.7 | | | | | | | | | | | 2.75724 | 0.09066 | 1.17988 |
| | | | | 0.5 | | | | | | | | | | 2.76382 | 0.16280 | 0.73671 |
| | | | | | 0.2 | | | | | | | | | 2.75837 | 0.10239 | 1.55071 |
| | | | | | | 1.0 | | | | | | | | 2.92871 | 0.03578 | 1.08039 |
| | | | | | | | 1.0 | | | | | | | 2.90893 | 0.04447 | 1.08124 |
| | | | | | | | | 1.2 | | | | | | 2.82801 | 0.27725 | 1.11324 |
| | | | | | | | | | 1.3 | | | | | 2.75613 | 0.09249 | 1.11714 |
| | | | | | | | | | | 1.0 | | | | 2.62265 | 0.12596 | 1.09129 |
| | | | | | | | | | | | 1.0 | | | 2.68129 | 0.10521 | 1.08834 |
| | | | | | | | | | | | | 0.7 | | 2.76032 | 0.26494 | 1.21211 |
| | | | | | | | | | | | | | 0.7 | 2.90532 | 0.05809 | 1.08205 |
| | | | | | | | | | | | | | | | | |
| | | | | | | | | | | | | | | | | |